# Influence of an imperfect energy profile on a seeded free electron laser performance

Botao Jia and Ying K. Wu
*Department of Physics, Duke University, Durham, North Carolina 27708-0305, USA,*
*and Duke Free Electron Laser Laboratory, Triangle Universities Nuclear Laboratory, Durham, North Carolina 27708-0308, USA*

Joseph J. Bisognano
*Synchrotron Radiation Center, University of Wisconsin-Madison, Stoughton, Wisconsin 53589, USA*

Alexander W. Chao and Juhao Wu*
*SLAC National Accelerator Laboratory, Menlo Park, California 94025, USA*
(Received 8 February 2010; published 16 June 2010)

A single-pass high-gain x-ray free electron laser (FEL) calls for a high quality electron bunch. In particular, for a seeded FEL amplifier and for a harmonic generation FEL, the electron bunch initial energy profile uniformity is crucial for generating an FEL with a narrow bandwidth. After the acceleration, compression, and transportation, the electron bunch energy profile entering the undulator can acquire temporal nonuniformity. We study the influence of the electron bunch initial energy profile nonuniformity on the FEL performance. Intrinsically, for a harmonic generation FEL, the harmonic generation FEL in the final radiator starts with an electron bunch having energy modulation acquired in the previous stages, due to the FEL interaction at those FEL wavelengths and their harmonics. The influence of this electron bunch energy nonuniformity on the harmonic generation FEL in the final radiator is then studied.

DOI: 10.1103/PhysRevSTAB.13.060701 PACS numbers: 41.60.Cr, 42.55.Vc, 42.65.Ky

## I. INTRODUCTION

The free electron laser (FEL) is perceived as one of the candidates for the fourth generation light source. Success in commissioning the world's first x-ray (1.5–15 Å) FEL—the LINAC Coherent Light Source (LCLS)—at SLAC National Accelerator Laboratory opens the gate for new science [1]. Further improving the FEL spectrum bandwidth is urged by various potential users. One of the possibilities to generate narrow bandwidth FEL is to invoke a coherent seed laser to start the FEL process, which is generally referred to as a seeded FEL. With a coherent seed laser, the radiator can set to have the resonant wavelength the same as the seed laser to simply form a FEL amplifier or an optical klystron (OK) [2]. An OK has two undulators with a magnetic buncher in between. For an OK, indeed the radiator can have the resonant frequency as one of the harmonics of the seed laser. In such an operation mode, a harmonic generation free electron laser (HGFEL) can be configured [3,4]. Because of the fact that the buncher between the two undulators will rotate the phase space on the seed wavelength scale, the electron bunch entering the radiator will have multifrequency components in its energy spectrum. We investigate its impact on the radiator FEL performance, in particular the FEL bandwidth from this multifrequency energy spectrum. In general, the electron bunch generated from the photoinjector has a very small energy spread and small emittance. During the acceleration, bunch compression, and transportation, the electron bunch will experience the rf curvature, the second-order effect in the chicane, and collective effects, which will all lead to a nonuniform energy profile [5]. In addition, the electron bunch is subject to microbunching instability [6–13]. Thus, the electron bunch entering the undulator can have an energy modulation with multiple frequencies. Such energy modulation will impact the FEL performance and affect the FEL bandwidth. As mentioned above, there is interest in this subject because of the general attention to the problem of increasing the temporal coherence properties of single-pass short wavelength FEL sources. The seeded FEL can start the FEL process with a coherent laser seed; yet, the nonuniform beam energy profile along the electron bunch, which changes the resonance condition and the local gain factor driving part of the beam out of resonance, is one of the causes of degradation of the coherence length during the amplification process. Hence, the flatness requirement of the beam parameters for the operation of a seeded FEL was addressed [14], with the idea of reverse tracking the particles dynamics in order to provide a ''flat'' beam in the sense of uniform parameters at the entrance of the undulator. Along this line of thinking, the dynamical problem of the interaction of a seeded FEL with an energy chirped (linear and second-order) electron beam was also addressed [15–18].

A study conducted for single frequency energy modulation was recently reported [19]. In this paper, we consider multifrequency initial energy modulation which is closer to

*Corresponding author.
jhwu@SLAC.Stanford.EDU

 

the reality as we described above. We study the influence of the energy profile nonuniformity on the free electron laser (FEL) performance for a FEL amplifier as well as for a harmonic generation (HG) FEL. The theory is compared to three-dimensional simulation with GENESIS [20].

The paper is organized as follows. In Sec. II, the theory frame is laid out. We formulate it as an initial value problem within the Vlasov-Maxwell coupled equation framework. The seeded FEL evolution with an electron bunch having an initial multifrequency energy spectrum is derived. The FEL bandwidth with such a nonuniform energy profile electron bunch is computed and compared to that of an ideal monoenergetic electron bunch. The expression is cross-checked with GENESIS numerical simulation in Sec. III. In Sec. IV, we then discuss the impact of the electron bunch multifrequency energy spectrum on the harmonic generation FEL performance in the radiator. As mentioned above, intrinsically, a HGFEL in the radiator starts from an electron bunch with multifrequency energy spectrum. Some discussion is drawn in Sec. V.

## II. VLASOV-MAXWELL ANALYSIS FOR AN INITIAL VALUE PROBLEM

For a FEL amplifier, the FEL process starts from a coherent seed; while for an optical klystron [2] and (high-gain) harmonic generation FEL [4,21,22], the FEL radiation in the radiator starts from coherent emission from a microbunched electron bunch. Nevertheless, the coherent emission once generated will be decomposed into the FEL guided modes and will be amplified due to the same FEL process. The FEL amplification process by an electron bunch with multifrequency energy spectrum is the same and applicable to all these different FEL configurations. Hence, in the following let us formulate the FEL start-up and evolution process when the electron bunch has energy nonuniformity. We will postpone the discussion of the coherent emission for an optical klystron or a harmonic generation FEL in Sec. IV.

To analyze the start-up of a seeded FEL amplifier, we use the coupled set of Vlasov and Maxwell equations which describes the evolution of the electrons and the radiation fields [15]. This approach is used as well for the self-amplified spontaneous emission (SASE) FEL [23]. We will work with a one-dimensional system in this section.

### A. Vlasov-Maxwell equations

We follow the analysis and notation of Refs. [15,23]. Dimensionless variables are introduced as $Z = k_w z$, $\theta = (k_0 + k_w)z - \omega_0 t$, where $k_0 = 2\pi/\lambda_0$, $\omega_0 = k_0 c$, and $k_w = 2\pi/\lambda_w$ with $\lambda_0$ being the radiation wavelength, $\lambda_w$ being the undulator period, and $c$ being the speed of light in vacuum. We also introduce $p = 2(\gamma - \gamma_0)/\gamma_0$ as the measure of energy deviation, with $\gamma$ the Lorentz factor of an electron in the electron bunch, and $\gamma_0$ the resonant energy defined by $\lambda_0 = \lambda_w(1 + K^2/2)/(2\gamma_0^2)$, for a planar undulator, where the undulator deflecting parameter $K \approx 93.4 B_w \lambda_w$ with $B_w$ the peak magnetic field in Tesla and $\lambda_w$ the undulator period in meter. The electron distribution function $\psi(\theta, p, Z)$ is normalized, i.e., $\int \psi(\theta, p, Z) d\theta dp = 1$, with $\psi_0(\theta, p, Z)$ describing the slow-varying unperturbed component. The FEL electric field is written as $E(t, z) = A(\theta, Z)e^{i(\theta - Z)}$ with $A(\theta, Z)$ being the slow-varying envelope function.

The one-dimensional linearized Vlasov-Maxwell equations are

$$\frac{\partial \psi}{\partial Z} + p\frac{\partial \psi}{\partial \theta} - \frac{2D_2}{\gamma_0^2}(Ae^{i\theta} + A^* e^{-i\theta})\frac{\partial \psi_0}{\partial p} = 0 \quad (1)$$

and

$$\left(\frac{\partial}{\partial Z} + \frac{\partial}{\partial \theta}\right)A(\theta, Z) = \frac{D_1}{\gamma_0} e^{-i\theta} \int dp\, \psi(\theta, p, Z), \quad (2)$$

where in SI units $D_1 = e a_w n_0 [JJ]/(2\sqrt{2} k_w \varepsilon_0)$ and $D_2 = e a_w [JJ]/(\sqrt{2} k_w m c^2)$, with $e$ and $m$ being the charge and mass of the electron; $\varepsilon_0 \approx 8.85 \times 10^{-12}$ F/m being the vacuum permittivity; $n_0$ being the electron bunch density in units of $1/\mathrm{m}^3$; and $[JJ] = J_0[a_w^2/2(1 + a_w^2)] - J_1[a_w^2/2(1 + a_w^2)]$, where the dimensionless rms undulator parameter $a_w \equiv K/\sqrt{2}$ and $J_0(x)$ and $J_1(x)$ are the zeroth and first order Bessel functions. Equation (1) gives a general solution as

$$\begin{aligned}\psi(\theta, Z, p) \approx\ & \psi_0(\theta - pZ) + \int_0^Z dZ' \frac{2D_2}{\gamma_0^2} \\ & \times A[\theta - p(Z - Z')] e^{i[\theta - p(Z - Z')]} \\ & \times \frac{\partial \psi_0[\theta - p(Z - Z')]}{\partial p}. \end{aligned} \quad (3)$$

Plugging Eq. (3) into Eq. (2), we have

$$\begin{aligned}\left(\frac{\partial}{\partial Z} + \frac{\partial}{\partial \theta}\right)A(\theta, Z) =\ & \frac{D_1}{\gamma_0} e^{-i\theta} \int dp\, \psi_0(\theta - pZ) \\ & + (2\rho)^3 e^{-i\theta} \int dp \int_0^Z dZ' \\ & \times A[\theta - p(Z - Z')] \\ & \times e^{i[\theta - p(Z - Z')]} \frac{\partial \psi_0[\theta - p(Z - Z')]}{\partial p}, \end{aligned} \quad (4)$$

with $(2\rho)^3 \equiv (2D_1 D_2)/\gamma_0^3$ defining the FEL parameter $\rho$ [24,25].

### B. Initial energy imperfectness—General solution

To model an energy imperfectness in the electron bunch coming into the undulator, we assume that the initial energy distribution function is

$$\psi_0 = \delta[p + g(\theta_0)] = \delta[p + g(\theta - pZ)], \quad (5)$$

where $g(\theta_0)$ is a general function, and $\delta(x)$ is the Dirac delta function.

The Maxwell equation is further rewritten after performing a partial integral, as

$$\left(\frac{\partial}{\partial Z}+\frac{\partial}{\partial\theta}\right)A(\theta,Z)\approx\frac{D_1}{\gamma_0}\sum_j e^{-i\theta_j+ig(\theta_j)Z}\delta(\theta-\theta_j)\times\left\{+\frac{D_1}{\gamma_0}B(\theta-pZ)\right\}+i(2\rho)^3\int_0^Z dZ'(Z-Z')\times e^{ig(\theta)(Z-Z')}A(\theta,Z'),\tag{6}$$

where the initial discrete radiators (electrons) are modeled as $\sum_j\delta(\theta-\theta_j)\delta[p+g(\theta_j)]$ for the longitudinal coordinates following Eq. (5). This term is for modeling the shot noise which is responsible for the SASE FEL. In addition, we also introduce a component $B(\theta, Z)$, which is related to the bunching factor, $b$, as

$$b\equiv\left|\frac{1}{2\pi}\int_{-\pi}^{\pi}d\theta\int dp e^{-i\theta}\psi_0(\theta,p)\right|\equiv\left|\frac{1}{2\pi}\int_{-\pi}^{\pi}d\theta B(\theta)\right|.\tag{7}$$

This second term (given in the curly brackets) is written separately for a premicrobunched electron bunch. As written explicitly, after integration over $\theta$, the second term shows the evolution of the initial bunching factor following the pendulum equation, i.e., the bunch factor $b(Z)$ is a function of $Z$.

To further work on Eq. (6), we now introduce the Laplace transform,

$$f(\theta,s)=\int_0^\infty dZe^{-sZ}A(\theta,Z).\tag{8}$$

Likewise, we introduce

$$\tilde{B}(\theta,s)=\int_0^\infty dZe^{-sZ}B(\theta,Z),\tag{9}$$

for the premicrobunched component.

With this, Eq. (6) is now cast in the frequency domain as

$$\frac{\partial f(\theta,s)}{\partial\theta}+\left(s-\frac{i(2\rho)^3}{[s-ig(\theta)]^2}\right)f(\theta,s)=A(\theta,0)\left\{+\frac{D_1}{\gamma_0}\tilde{B}(\theta,s)\right\}+\frac{D_1}{\gamma_0}\sum_j\frac{e^{-i\theta_j}\delta(\theta-\theta_j)}{s-ig(\theta_j)},\tag{10}$$

which yields the general solution as

$$f(\theta,s)=f(-\infty,s)+\int_{-\infty}^{\theta}d\theta' e^{-s(\theta-\theta')+\int_{\theta'}^{\theta}\{i(2\rho)^3/[s-ig(\theta'')]^2\}d\theta''}\times\left[A(\theta',0)\left\{+\frac{D_1}{\gamma_0}\tilde{B}(\theta',s)\right\}+\frac{D_1}{\gamma_0}\sum_j\frac{e^{-i\theta_j}\delta(\theta'-\theta_j)}{s-ig(\theta_j)}\right].\tag{11}$$

Notice that, in the square brackets in Eq. (11), the first term $A(\theta, 0)$ characterizes the initial seed for a seeded FEL, the second term models a premicrobunched electron bunch, while the third term models the SASE FEL. In the following, let us focus on a seeded FEL, so that the second term and third term in the square brackets will be ignored in the derivation.

### C. Initial energy modulation—An example

In this section, the general function $g(\theta)$ as in Eq. (5) characterizing the nonuniform energy profile is represented as a Fourier series as in the following. Indeed, for electron bunch experienced microbunching instability, or in the harmonic generation FEL as explained above and detailed in the following Sec. IV B, there can be an energy modulation along the electron bunch as

$$\gamma=\gamma_0+\sum_{m=1}^{\infty}\varepsilon_m\sin[\omega_m(t-t_0)],\tag{12}$$

where $\omega_m$ characterizes the $m$th component of the energy modulation. The initial energy distribution function is then

$$\psi_0=\delta\left[p+\sum_{m=1}^{\infty}\eta_m\sin(\omega_{\eta_m}\theta_0)\right],\tag{13}$$

where $\eta_m\equiv 2\varepsilon_m/\gamma_0$ and $\omega_{\eta_m}\equiv\omega_m/\omega_0$. For such a sinusoidal modulation, we have

$$\int_{\theta'}^{\theta}\frac{i(2\rho)^3}{[s-i\sum_{m=1}^{\infty}\eta_m\sin(\omega_{\eta_m}\theta'')]^2}d\theta''\approx\frac{i(2\rho)^3(\theta-\theta')}{s^2}+\sum_{m=1}^{\infty}\frac{2\eta_m(2\rho)^3[\cos(\omega_{\eta_m}\theta)-\cos(\omega_{\eta_m}\theta')]}{\omega_{\eta_m}s^3},\tag{14}$$

to the leading order in $\eta_m$.

#### 1. The FEL solution

For a seeded FEL, let us throw away the initial value term, the premicrobunched term, as well as the SASE term, and keep only the seed in Eq. (11):

$$f(\theta,s)\approx\int_{-\infty}^{\theta}d\theta' A(\theta',0)e^{-s(\theta-\theta')+[i(2\rho)^3(\theta-\theta')/s^2]+\sum_{m=1}^{\infty}\{2\eta_m(2\rho)^3[\cos(\omega_{\eta_m}\theta)-\cos(\omega_{\eta_m}\theta')]/(\omega_{\eta_m}s^3)\}}.\tag{15}$$

The inverse Laplace transform then gives us the FEL electric field slow-varying envelope function as

$$A(\theta, Z) = \int_c \frac{ds}{2\pi i} e^{sZ} f(\theta, s) \approx \int_c \frac{ds}{2\pi i} e^{sZ} \int_{-\infty}^{\theta} d\theta' A(\theta', 0) e^{-s(\theta-\theta')+[i(2\rho)^3(\theta-\theta')/s^2]+\sum_{m=1}^{\infty}\{2\eta_m(2\rho)^3[\cos(\omega_{\eta_m}\theta)-\cos(\omega_{\eta_m}\theta')]/(\omega_{\eta_m}s^3)\}}. \quad (16)$$

Obviously, once we know the initial seed field envelope $A(\theta, 0)$, we can obtain the seeded FEL field envelope $A(\theta, Z)$ along the undulator.

The double integral in Eq. (16) can be evaluated by first performing the contour integral to get

$$A(\theta, Z) = \int_0^{\infty} d\xi A(\theta - \xi, 0) \mathcal{G}(\theta, \xi, Z, s, \eta), \quad (17)$$

with the Green function $\mathcal{G}(\theta, \xi, Z, s, \eta)$ and the corresponding phasor $\mathcal{F}(\theta, \xi, Z, s, \eta)$ defined as

$$\mathcal{G}(\theta, \xi, Z, s, \eta) \equiv \int_c \frac{ds}{2\pi i} e^{s(Z-\xi)+[i(2\rho)^3\xi/s^2]+\sum_{m=1}^{\infty}(2\eta_m(2\rho)^3\{\cos(\omega_{\eta_m}\theta)-\cos[\omega_{\eta_m}(\theta-\xi)]\}/[\omega_{\eta_m}s^3])} \equiv \int_c \frac{ds}{2\pi i} \exp[\mathcal{F}(\theta, \xi, Z, s, \eta)], \quad (18)$$

where $\eta = \{\eta_1, \eta_2, \ldots, \eta_\infty\}$. In Eq. (17), we implicitly introduce $\xi \equiv \theta - \theta'$. The Green function can be estimated by saddle point approximation. The saddle point $s_s$ is found from

$$\left.\frac{d\mathcal{F}(\theta, \xi, Z, s, \eta)}{ds}\right|_{s=s_s} = 0, \quad (19)$$

and the Green function is approximated as

$$\mathcal{G}(\theta, \xi, Z, s, \eta) \approx \frac{\exp[\mathcal{F}(\theta, \xi, Z, s_s, \eta)]}{[2\pi\mathcal{F}''(\theta, \xi, Z, s_s, \eta)]^{1/2}} \cong \frac{-e^{i\pi/12}}{\sqrt{2\pi Z/\rho}} e^{i^{1/3}2\rho Z-[i^{1/3}9(\theta-Z/3)^2\rho/(2Z)]-\sum_{m=1}^{\infty}(i2\eta_m\{\cos(\omega_{\eta_m}\theta)-\cos[\omega_{\eta_m}(\theta-\xi)]\}/\omega_{\eta_m})}. \quad (20)$$

For an initial Gaussian seed, we model it as

$$E(t, z=0) = E_0 e^{-i\omega_0 t-\alpha_0 t^2} = E_0 e^{i\theta-\theta^2\alpha_0/\omega_0^2} \Rightarrow A(\theta, 0) = E_0 e^{-\theta^2\alpha_0/\omega_0^2}, \quad (21)$$

where $\alpha_0 = 1/(4\sigma_{t0}^2)$ with $\sigma_{t0}$ being the initial seed rms pulse duration. According to Eq. (17), the FEL pulse is

$$\begin{aligned} A(\theta, Z) &= E_0 \frac{-e^{i\pi/12}}{\sqrt{2\pi Z/\rho}} e^{i^{1/3}2\rho Z-[i^{1/3}9(\theta-Z/3)^2\rho/(2Z)]-\sum_{m=1}^{\infty}[i2\eta_m\cos(\omega_{\eta_m}\theta)/\omega_{\eta_m}]} \int_{-\infty}^{\theta} d\theta' e^{-(\theta'^2\alpha_0/\omega_0^2)+\sum_{m=1}^{\infty}[i2\eta_m\cos(\omega_{\eta_m}\theta')/\omega_{\eta_m}]} \\ &\approx E_0\omega_0 \frac{-e^{i\pi/12}}{\sqrt{2\alpha_0 Z/\rho}} \left(1 + \sum_{m=1}^{\infty} \frac{i2\eta_m}{\omega_{\eta_m}} e^{-[\omega_0^2\omega_{\eta_m}^2/(4\alpha_0)]}\right) e^{i^{1/3}2\rho Z-[i^{1/3}9(\theta-Z/3)^2\rho/(2Z)]-\sum_{m=1}^{\infty}[i2\eta_m\cos(\omega_{\eta_m}\theta)/\omega_{\eta_m}]} \\ &\approx E_0\omega_0 \frac{-e^{i\pi/12}}{\sqrt{2\alpha_0 Z/\rho}} e^{i\chi} e^{i^{1/3}2\rho Z-[i^{1/3}9(\theta-Z/3)^2\rho/(2Z)]-\sum_{m=1}^{\infty}[i2\eta_m\cos(\omega_{\eta_m}\theta)/\omega_{\eta_m}]}. \end{aligned} \quad (22)$$

where

$$\chi = \sum_{m=1}^{\infty} \frac{2\eta_m}{\omega_{\eta_m}} e^{-[\omega_0^2\omega_{\eta_m}^2/(4\alpha_0)]}. \quad (23)$$

It is interesting to find that to the first order in $\eta$, in the exponential function, the microbunching energy modulation only leads to a pure phase modulation, but does not affect the power. To see this more explicitly, one can exponentiate the small correction term $\sum_{m=1}^{\infty}(i2\eta_m/\omega_{\eta_m})\exp[-\omega_0^2\omega_{\eta_m}^2/(4\alpha_0)]$ in front of the exponential function as we show above.

### 2. Bandwidth

As we find above, the first order correction is a pure phase modulation; we would like to investigate this phase modulation on the FEL coherence. Recall that one of the most important purposes of a seeded FEL is to generate transform limited light; let us now find the FEL spectrum:

$$\tilde{E}(\omega, z) \equiv \frac{1}{\sqrt{2\pi}} \int dt E(t, z) e^{i\omega t}. \quad (24)$$

Notice that $E(t, z) \sim e^{-i\omega_0 t}$, hence the Fourier transform is defined as in Eq. (24).

First, we rewrite $E(t, z)$ to have $t$ dependence explicit, i.e.,

$$E(t,z) \approx E_0\omega_0 \frac{-e^{i\pi/12}}{\sqrt{2\alpha_0 Z/\rho}} e^{i\chi} e^{ik_0 Z/k_w - 6i^{1/3}k_0\rho Z/k_w - 9i^{1/3}k_0^2\rho Z/(2k_w^2)} e^{[9i^{1/3}\rho\omega_0/(v_g k_w)-i]\omega_0 t - 9i^{1/3}\rho\omega_0^2 t^2/(2Z)}$$
$$\times\left[1 - \sum_{m=1}^{\infty} \frac{i\eta_m}{\omega_{\eta_m}}(e^{i\omega_{\eta_m}\theta} + e^{-i\omega_{\eta_m}\theta})\right]$$
$$\equiv \mathcal{A}(z) e^{[9i^{1/3}\rho\omega_0/(v_g k_w)-i]\omega_0 t - 9i^{1/3}\rho\omega_0^2 t^2/(2Z)}\left[1 - \sum_{m=1}^{\infty} \frac{i\eta_m}{\omega_{\eta_m}}(e^{i\omega_{\eta_m}\theta} + e^{-i\omega_{\eta_m}\theta})\right]$$
$$\equiv \mathcal{A}(z) e^{i^{1/3}\mathcal{B}z^2/v_g^2} e^{-i\omega_0 t - i^{1/3}\mathcal{B}(t-z/v_g)^2}\left[1 - \sum_{m=1}^{\infty} \frac{i\eta_m}{\omega_{\eta_m}}(e^{i\omega_{\eta_m}\theta} + e^{-i\omega_{\eta_m}\theta})\right], \tag{25}$$

where $v_g \equiv \omega_0/(k_0 + 2k_w/3)$ is the FEL group velocity for a coasting beam without energy nonuniformity [15,23,26,27], and $\mathcal{B} = 9\rho\omega_0^2/(2Z)$.

Completing the integral in Eq. (24), we have

$$\tilde{E}(\omega, z) = \frac{\mathcal{A}(z)}{\sqrt{2\mathcal{B}i^{1/3}}} e^{i^{5/3}[(\omega-\omega_0)-(2i^{4/3}\mathcal{B}z/v_g)]^2/(4\mathcal{B})}\left\{1 - \sum_{m=1}^{\infty} \frac{2i\eta_m}{\omega_{\eta_m}} e^{i^{5/3}\omega_0^2\omega_{\eta_m}^2/(4\mathcal{B})} \cos\left[\frac{\omega_{\eta_m} k_w z}{3} - \frac{i^{2/3}(\omega-\omega_0)\omega_0\omega_{\eta_m}}{2\mathcal{B}}\right]\right\}. \tag{26}$$

For the following calculation, the FEL energy density is then introduced as

$$\mathcal{I}(\omega, z) \equiv \tilde{E}(\omega, z)\tilde{E}^*(\omega, z), \tag{27}$$

where $\tilde{E}^*(\omega, z)$ is the complex conjugate of $\tilde{E}(\omega, z)$.

With this FEL energy density function, we can compute the FEL average frequency as

$$\langle\omega(z)\rangle \equiv \frac{\int \omega \mathcal{I}(\omega, z) d\omega}{\int \mathcal{I}(\omega, z) d\omega} \approx \omega_0\left\{1 + \sum_{m=1}^{\infty} 2\eta_m e^{-[(\omega_0^2\omega_{\eta_m}^2)/(4\sqrt{3}\mathcal{B})]} \sin(\omega_{\eta_m} z k_w/3)\right\}. \tag{28}$$

So, we see clearly how the energy nonuniformity can drive part of the beam out of the resonant to the seed laser as mentioned in Sec. I. To characterize the influence more quantitatively, we now compute the standard deviation, which is

$$\sigma_\omega(z) \equiv \sqrt{\frac{\int \omega^2 \mathcal{I}(\omega, z) d\omega}{\int \mathcal{I}(\omega, z) d\omega} - [\langle\omega(z)\rangle]^2} \approx \frac{2\mathcal{B} - \sum_{m=1}^{\infty} \eta_m \omega_0^2 \omega_{\eta_m} e^{-[\omega_0^2\omega_{\eta_m}^2/(4\sqrt{3}\mathcal{B})]} \cos(\omega_{\eta_m} z k_w/3)}{\sqrt{2\sqrt{3}\mathcal{B}}}$$
$$\equiv \frac{2\mathcal{B} - \sum_{m=1}^{\infty} \mathcal{C}_m \cos(\omega_{\eta_m} z k_w/3)}{\sqrt{2\sqrt{3}\mathcal{B}}} \equiv \frac{2\mathcal{B} + \sum_{m=1}^{\infty} \mathcal{D}_m}{\sqrt{2\sqrt{3}\mathcal{B}}}. \tag{29}$$

Notice that, for $\eta = 0$,

$$\sigma_\omega(z)|_{\eta=0} \equiv \sigma_{\omega,0}(z) \overset{1-\mathrm{D}}{=} \omega_0\sqrt{\frac{3\sqrt{3}\rho}{k_w z}} \tag{30}$$

is the well-known 1D rms bandwidth of the FEL Green function for a coasting electron beam without energy nonuniformity [23,26,27].

To be explicit, we have

$$\left|\frac{\mathcal{D}_m}{2\mathcal{B}}\right| = \frac{\eta_m \omega_{\eta_m} k_w z}{9\rho} e^{-[(\omega_{\eta_m}^2 k_w z)/(18\sqrt{3}\rho)]} |\cos(\omega_{\eta_m} z k_w/3)|. \tag{31}$$

Recall that $\omega_{\eta_m} = \omega_m/\omega_0$ is the ratio of the $m^{th}$ component microbunching frequency to the FEL frequency. Before we give a detailed study in the following, let us look at an example. For LCLS 1.5 Å FEL [1], the undulator period $\lambda_w = 3$ cm and the FEL parameter $\rho \sim 5.0 \times 10^{-4}$ for nominal operation. The microbunching instability has peak gain modulation with period around 0.5 $\mu$m entering the undulator. Assuming $\eta_m = 0.2\rho$, Eq. (31) predicts about 10% bandwidth increment due to this energy modulation along the undulator.

For a cascaded high-gain harmonic generation FEL [28], the most serious degradation will be at the first stage, where the FEL frequency is the lowest. This is due to the $n^2$ amplification of any degradation from the first stage into the final FEL radiation, assuming that we are doing $n^{\text{th}}$ harmonic generation. So, the first stage degradation is always the most severe one regarding this imperfectness and also shot noise [29,30].

We make some general comments here. First, we rewrite the oscillation phase in Eq. (31) as

$$\omega_{\eta_m} z k_w/3 = \frac{1}{6\sqrt{3}} \frac{z}{L_G^{1D}} \frac{\omega_{\eta_m}}{\rho}, \tag{32}$$

where the 1D power gain length is defined as

$$L_G^{1D} \equiv \frac{\lambda_w}{4\sqrt{3}\pi\rho}. \tag{33}$$

So, if $\omega_{\eta_m}$ is a few times larger than $\rho$, then during the exponential growth region, i.e., $z$ can be up to about $20L_G^{1D}$, this $\cos(\omega_{\eta_m} z k_w/3)$ term can lead to a few oscillations. In this case, the $\exp[-\omega_{\eta_m}^2 k_w z/(18\sqrt{3}\rho)]$ term will exponentially decrease quickly along the undulator $z$ making the overall degradation small along the undulator. So, it is worthwhile to study when the phase is not too large. In that case, let us simply look at the oscillation amplitude only, i.e., we can study $\mathcal{C}_m/(2\mathcal{B})$, which is maximum at

$$z = \frac{18\sqrt{3}\rho}{k_w \omega_{\eta_m}^2} = 108 L_G^{1D} \frac{\rho^2}{\omega_{\eta_m}^2}. \tag{34}$$

At this location defined in Eq. (34), we have

$$\frac{\mathcal{C}_m}{2\mathcal{B}} = \frac{2\sqrt{3}\eta_m}{\omega_{\eta_m}} e^{-1}. \tag{35}$$

One can also find that the bandwidth degradation is maximized for

$$\omega_{\eta_m} = 3^{5/4} \sqrt{\frac{\rho}{k_w z}} = 3\sqrt{6}\rho \sqrt{\frac{L_G^{1D}}{z}}. \tag{36}$$

That said, we expect the bandwidth degradation to be small for both $\omega_{\eta_m}$ small and large limits. We will explore this more in Sec. III. For this particular energy modulation frequency defined in Eq. (36), we have

$$\frac{\mathcal{C}_m}{2\mathcal{B}} = \frac{1}{3\sqrt{2}} \frac{\eta_m}{\rho} \sqrt{\frac{z}{L_G^{1D}}} e^{-1/2}. \tag{37}$$

Of course, with the oscillation term as in Eq. (31), more detailed analysis is needed for discussion of the maximum degradation. We prefer not to analytically elaborate it more here, but rather leave the discussion to Sec. III.

## III. SIMULATION

In this section, we would like to compare the analytical calculations with numerical simulations. The simulations are carried out by GENESIS working in time dependent mode [20]. The bandwidth degradation shown by our theory is quantitatively measured by the bandwidth degradation which is defined as

$$\Delta\sigma_\omega(z) \equiv \left| \frac{\sigma_\omega(z) - \sigma_{\omega,0}(z)}{\sigma_{\omega,0}(z)} \right|, \tag{38}$$

where $\sigma_{\omega,0}(z)$ is the FEL bandwidth with perfect monoenergetic initial electron beam energy $\varepsilon_m = 0$, $\sigma_\omega(z)$ is bandwidth with modulated initial beam energy, and the degradation $\Delta\sigma_\omega(z)$ is the absolute value of the relative ratio as defined in Eq. (38).

TABLE I. Parameters for simulation.

| Parameters | Value |
|---|---|
| RMS undulator parameter ($a_w$) | 1.4 |
| Undulator wavelength ($\lambda_w$) | 0.02 m |
| Period for each undulator ($N_u$) | 300 |
| Resonant energy ($\gamma_0$) | 502 |
| Initial energy rms spread ($\sigma_\gamma/\gamma_0$) | $10^{-5}$ |
| Initial peak current ($I_{\text{peak}}$) | 800 A |
| Normalized rms $X$ emittance | 2.9 mm mrad |
| Normalized rms $Y$ emittance | 2.9 mm mrad |
| Resonant wavelength ($\lambda_0$) | 118.4 nm |
| Scaled beam size ($\tilde{a}$) | 3.29 |
| FEL parameter ($\rho$) | 0.0043 |
| 1D power gain length ($L_G^{1D}$) | 0.21 m |

In order to compare with the theory, proper simulation configurations have to be carefully set. The theory is in accord with the high-gain FEL situation so the FEL characteristic parameter $\rho$ could not be small compared to electron bunch intrinsic energy spread. On the other hand, as shown in Eq. (29), the degradation is characterized by the oscillations with period of $3\lambda_w/\omega_{\eta_m}$, so in order to have a few oscillations in the exponential growth region, $\rho$ could neither be so large that saturation happens too soon. In addition, the modulation $\eta_m$ of the initial beam energy should be large enough to overwhelm the internal numerical simulation noise. Yet, $\eta_m$ should also be smaller than $\rho$, otherwise the FEL exponential growth is undermined. The parameters for the simulation are listed in Table I.

In Table I, we introduce a parameter $\tilde{a}$, whose square is defined as

$$\tilde{a}^2 \equiv 4\rho k_0 k_w r_0^2, \tag{39}$$

where $r_0$ is the transverse radius of the electron bunch assuming a transverse uniform hard edge distribution [31]. The parameter $\tilde{a}$ characterizes the 3D effects. Following Ref. [31], we will set $\tilde{a} \in (2, 6)$ in the following simulation. This is the interesting region where current designing or operating x-ray FEL projects sit. For example, for LCLS [1], $\tilde{a}$ is about 4. For $\tilde{a} \in (2, 6)$, the FEL power growth rate is close to 1D results and single mode dominates. Gain guiding is very effective and transverse coherence of the FEL mode is well achieved. So, this is the range where high-gain FELs are designed. Therefore, we will focus in this range to compare the theory with full 3D simulation.

We first show the bandwidth degradation of a single frequency electron bunch energy modulation. The theoretical calculation of the bandwidth curves $\sigma_{\omega,0}(z)$, $\sigma_\omega(z)$ and the degradation $\Delta\sigma_\omega(z)$ curves are shown in Fig. 1. The simulation bandwidth curves and the degradation curve are

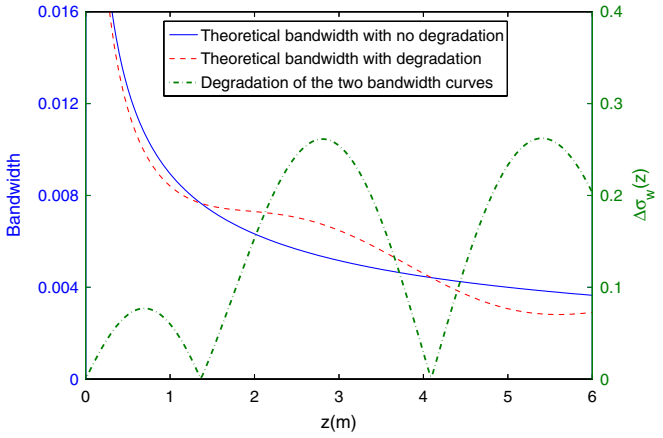


FIG. 1. (Color) Theoretical bandwidth curves and bandwidth degradation. Bandwidth curves are with perfect beam energy and modulated beam energy, respectively. The beam energy modulation for the degraded bandwidth curve is $\varepsilon_m = 0.6$, i.e., $\eta_m = 0.0024$. The theoretical calculation is based on the parameters listed in Table I.

shown in Fig. 2 as a comparison to the theoretical curves in Fig. 1.

As can be seen from Fig. 1, with imperfect initial beam energy, the bandwidth is oscillating around the nonmodulated one. This oscillation contributes to the degradation $\Delta\sigma_\omega(z)$ which is shown as a few consecutive humps. Figure 2 shows the simulation and compares the simulated degradation $\Delta\sigma_\omega(z)$ with the theory calculation. As can be seen, from about 1.9 m to about 3.6 m, $\Delta\sigma_\omega(z)$ of the simulation and the theory are in accord with each other reasonably well in terms of both pattern and value. The discrepancy outside of the (1.9, 3.6) m region is explained in Fig. 3.

As shown in Fig. 3, the simulation gain length are flat and close to the theoretical number within a certain region.

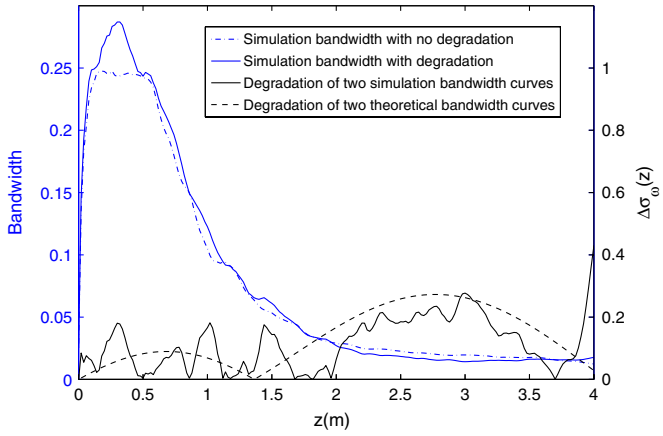


FIG. 2. (Color) Simulations of bandwidth curves and bandwidth degradation. The theoretical degradation curve is copied from Fig. 1. The beam energy modulation for the degraded bandwidth curve is the same as in Fig. 1. The simulation parameters are listed in Table I.

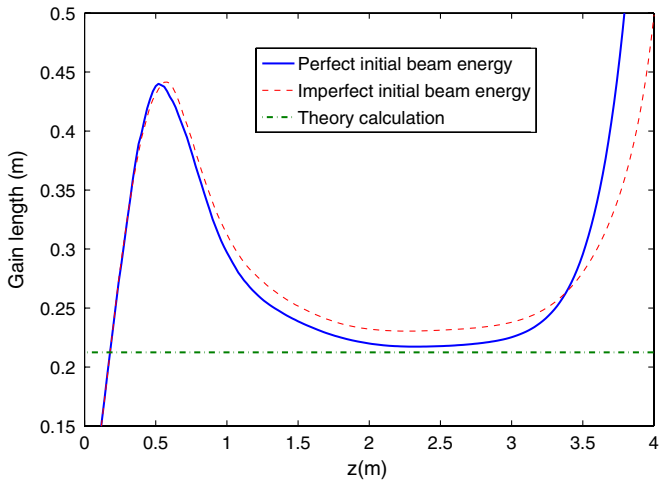


FIG. 3. (Color) Theoretical and simulation gain length curves. The theoretical gain length is a fixed number. The number is plotted as a straight line (dot-dashed) and extended horizontally. The solid curve and the dashed curve are the simulation gain length for perfect initial beam energy and modulated initial beam energy, respectively. The simulation parameters are the same as in Fig. 2 and listed in Table I.

Before 2 m and after 3.5 m, the gain length difference is huge so the theoretical $\Delta\sigma_\omega(z)$ does not follow the simulation curve well within this region as shown in Fig. 2. The region where the theory and simulation have discrepancy is either the start-up region or the saturation region. This is expected, since the theory is developed for the exponential growth region only. A similar situation is found for the case of multifrequency modulation as in Fig. 4. In Fig. 4, a

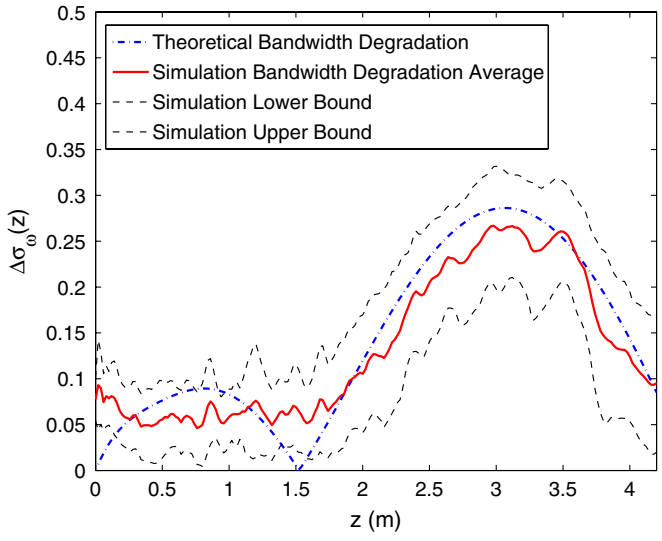


FIG. 4. (Color) Simulation and theory bandwidth degradation with multifrequency initial beam energy modulation. The beam energy modulation parameters are $\omega_m = (0.002, 0.04, 0.01)\omega_0$, $\epsilon_m = (0.05, 0.1, 0.6)$. The simulation parameters are listed in Table I. The red solid curve is the average of 20 simulation curves. The two black dashed boundary curves represent the simulation confidence intervals.

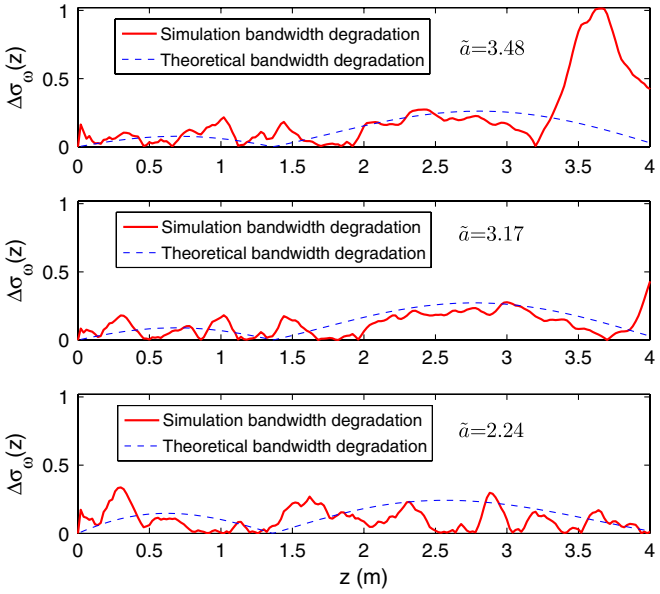


FIG. 5. (Color) Bandwidth degradation for different $\tilde{a}$. The initial beam energy modulation is $\epsilon_m = 0.6$, $\omega_m = 0.011 \times \omega_0$. The simulation parameters are listed in Table I, except $\tilde{a}$ and the initial peak current $I_{\text{peak}} = 1400$, 800, and 100 A for top, middle, and bottom pictures, respectively.

number of simulations are carried out to eliminate the impact of numeric noise. The simulation sample statistics such as the first- and the second-order moments are calculated; and the average simulated bandwidth degradation with confidence intervals is constructed accordingly. As can be seen, the theory and simulation agree with each other in the exponential growth region from 2.0 to 3.7 m within the confidence interval.

Our theory is a 1D theory which is valid when $\tilde{a}$ is large enough. In Fig. 5, we show series simulations with a few different values of $\tilde{a}$. It can be seen, at smaller $\tilde{a}$ ($\tilde{a} \to 2$) where the 1D limit is not achieved, the theory does not match the simulation. In addition, at a higher peak current, the FEL enters saturation faster so the top plot of Fig. 5 shows the bandwidth degradation follows the theory up to a shorter range before saturation starts.

In Sec. II C 2, we state that the degradation is small for both small and large $\omega_{\eta_m}$. In the single modulation frequency case, where $m = 1$ and Eq. (38) becomes Eq. (31), we plot Eq. (31) at a fix $z = 3$ m as a function of $\omega_{\eta_m}$ as shown in Fig. 6. Our theory predicts that the maximum bandwidth degradation is around $\omega_{\eta_m} = 0.01$ (following the parameters listed in Table I). Figure 7 shows the bandwidth degradation within the shaded area in Fig. 6. As can be seen in Fig. 7, around the peak of Fig. 6, degradations follow the theoretical prediction and at the boundaries of the shaded area, degradations start to vanish. Figure 8 shows the extreme cases where $\omega_{\eta_m}$ is either too large or too small. The simulation bandwidth degradation is dominated by noise which is expected.

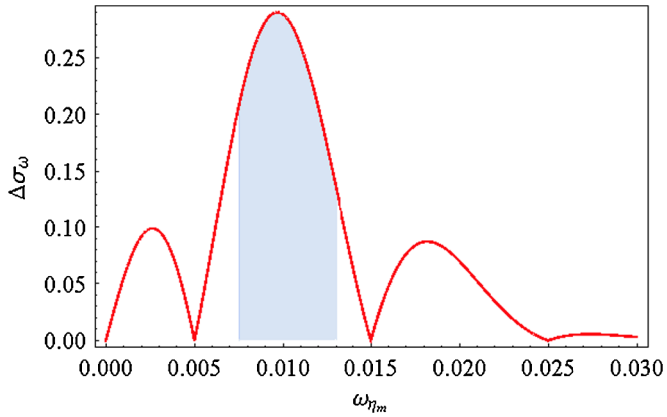


FIG. 6. (Color) Bandwidth degradation $\Delta\sigma_\omega(z)$ as a function of $\omega_{\eta_m}$ at $z = 3$ m. The simulation parameters are listed in Table I. Bandwidth degradation at the shaded area is shown in Fig. 7.

It can be noticed that there is a noise beating pattern for the simulations we have shown. The internal numerical noise of the simulation contributes to the noise beating. Figure 9 shows the bandwidth comparison of two simulations with perfect initial bunch energy. The calculation is done in the manner similar to Eq. (38). The curve shows the absolute value of the two bandwidth curve difference divided by one of the bandwidth curves. As can be seen,

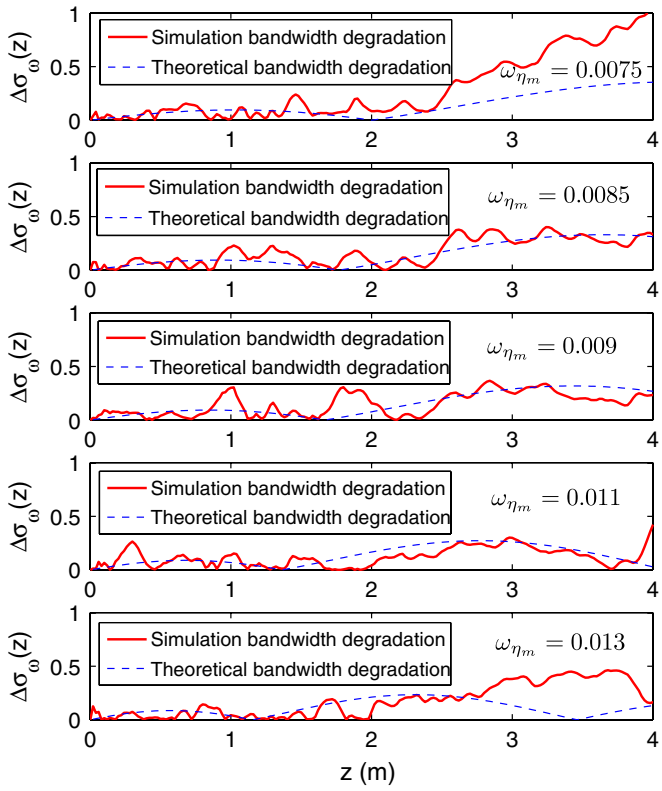


FIG. 7. (Color) Bandwidth degradation for different $\omega_{\eta_m}$. The simulation parameters are listed in Table I. The initial bunch energy modulation frequency $\omega_{\eta_m}$ is a single value for each plot.

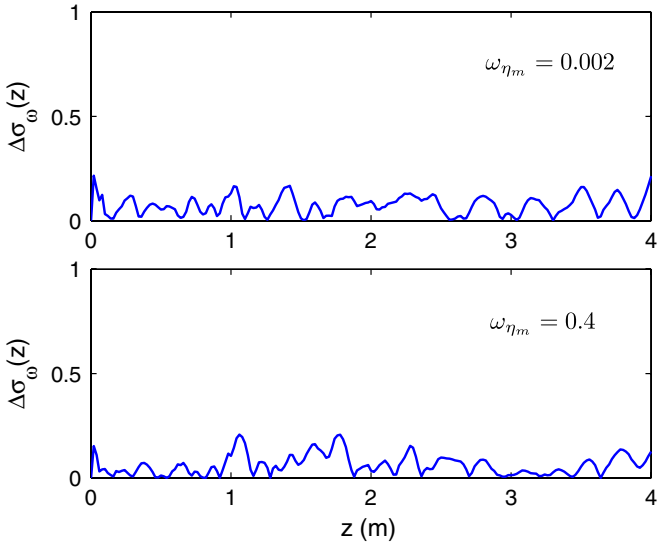


FIG. 8. (Color) Simulated bandwidth degradation for extremely small and large $\omega_{\eta_m}$. The simulation parameters are listed in Table I.

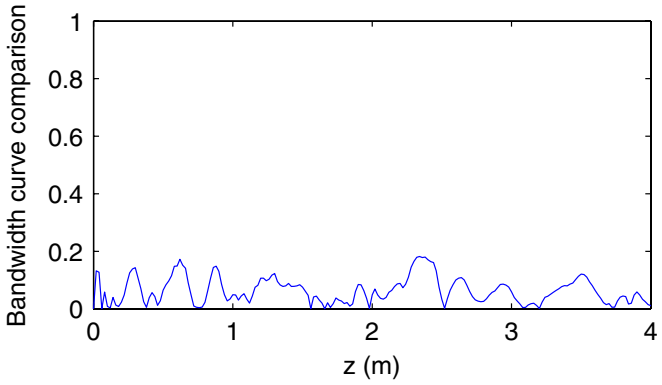


FIG. 9. (Color) The bandwidth difference from two simulations with no initial energy modulation and different random number generator seeds. The simulation parameters are listed in Table I.

different random number generator seeds could introduce the noise beating and the two bandwidth curves are not identical. This is also a measure of the statistical fluctuation of the numerical simulation, which is quite challenging itself.

## IV. IMPACT ON A SEEDED FEL

The work developed in the previous sections is sufficient to study the bandwidth degradation of a seeded FEL amplifier when the electron bunch has a nonuniform energy profile. Yet, for a harmonic generation FEL or an optical klystron configuration, there is no initial radiation seed, but rather the FEL will start from a premicrobunched electron bunch. In fact, this can be done by keeping the prebunched term (given in the curly brackets) and throwing away the seed term and the SASE term in Eq. (11). Therefore, Eq. (15) should be modified accordingly. The follow-up analysis will have to be modified as well. This is being reported in another publication. In the following, we will get the coherent radiation power and study the bandwidth degradation in the radiator treating the coherent radiation power as a seed.

### A. Coherent emission power

In the radiator of a HG FEL [3,4], the coherent radiation power of the premicrobunched electron bunch at the fundamental frequency is [22,32]

$$P_1^{\mathrm{coh}} = \frac{Z_0 b_l^2 N_e^2 e^2 \gamma^2 N_u^2}{4\sqrt{2}\sigma_t^2} \frac{1}{k_r^2 \sigma_\perp^2} \frac{K^2}{(1+\frac{K^2}{2})^2} \times \left[ J_1\left(\frac{K^2}{4+2K^2}\right) - J_0\left(\frac{K^2}{4+2K^2}\right)\right]^2, \quad (40)$$

where we assume that the radiator is resonant at the $l^{\mathrm{th}}$ harmonic of the modulator in a HG FEL with the corresponding bunching factor being $b_l$. This is the start-up power which is treated as the coherent seed. In Eq. (40), $Z_0$ is the vacuum impedance, $N_e$ is the number of electrons in the bunch, $N_u$ is the number of undulator periods, $k_r = 2\pi/\lambda_r$ with $\lambda_r$ being the radiator resonant wavelength, and $\sigma_\perp$ is the electron bunch transverse rms size.

### B. Electron energy profile into the radiator

Since we are working with a cold electron bunch without intrinsic energy spread, the phase space distribution function at the exit of the modulator in a HG FEL will be

$$\delta(\delta\gamma - \Delta\gamma \sin\theta), \quad (41)$$

where $\delta\gamma \equiv (\gamma - \gamma_0)/\gamma_0$ with $\gamma_0$ as the electron centroid energy, and $\delta(x)$ is the Dirac delta function. After the buncher, the phase space distribution is then

$$\delta\left[\delta\gamma - \Delta\gamma \sin\left(\theta - \frac{d\theta}{d\gamma}\delta\gamma - \theta_0\right)\right], \quad (42)$$

where $d\theta/d\gamma$ characterizes the buncher strength and $\theta_0$ for an overall phase shift.

Based on the reversion of series method [33], Eq. (42) yields a formal series expansion as

$$\delta\gamma = \sum_{n=1}^{\infty} \frac{\Delta\gamma^n}{n!} \frac{d^{n-1}\sin^n(-\frac{d\theta}{d\gamma}x + \theta - \theta_0)}{dx^{n-1}}\bigg|_{x=0}. \quad (43)$$

With this formal expression, $\delta\gamma$ is ready to be further expressed as a Fourier series,

$$\delta\gamma = \sum_{m=1}^{\infty} a_m \sin[m(\theta - \theta_0)] \equiv \sum_{m=1}^{\infty} a_m \sin(m\Theta), \quad (44)$$

where the Fourier coefficient is calculated as

$$a_m = \frac{1}{\pi}\int_{-\pi}^{\pi}\sum_{n=1}^{\infty}\frac{\Delta\gamma^n}{n!}\frac{d^{n-1}\sin^n(-\frac{d\theta}{d\gamma}x+\Theta)}{dx^{n-1}}\Big|_{x=0}\sin(m\Theta)d\Theta$$
$$= \frac{2}{\pi}\sum_{n=1}^{\infty}\frac{\Delta\gamma^n}{n!}\frac{1}{(2i)^{n+1}}\sum_{k=0}^{n}c_n^k(-)^{n-k}\left[i(2k-n)\left(-\frac{d\theta}{d\gamma}\right)\right]^{n-1}\left[\frac{e^{i(2k+m-n)\pi}-1}{i(2k+m-n)}-\frac{e^{i(2k-m-n)\pi}-1}{i(2k-m-n)}\right], \quad (45)$$

where $c_n^k$ is the binomial coefficient.

As mentioned above, assuming that the radiator is resonant at frequency $\omega_0$ which is the $l^{\text{th}}$ harmonic of the first undulator—the modulator—fundamental frequency, then we can rewrite Eq. (45) according to Eqs. (12) and (13). We have

$$\omega_m = \frac{m\omega_0}{l} \qquad \omega_{\eta_m} = \frac{m}{l} \qquad \varepsilon_m = a_m \qquad \eta_m = \frac{2a_m}{\gamma_0}. \quad (46)$$

Combining Eqs. (31) and (46), one can estimate the impact on the FEL bandwidth from the energy modulation generated in the modulator. As an example, assuming a seed laser with a wavelength of 240 nm, via HG FEL, the final FEL wavelength is $\lambda_0 = 4$ nm. Further assuming that the final 4 nm FEL has FEL parameter $\rho = 3.0\times10^{-3}$, undulator period of $\lambda_w = 5$ cm, and the generic energy modulation at 240 nm leads to $\eta_m = 0.3\rho$, then over the 10 m long undulator the bandwidth increment is about 5%.

## V. DISCUSSION

As a conclusion, in this paper, we study the effect on a seeded FEL amplifier performance due to an initial energy nonuniformity when the electron bunch enters the undulator. Such nonuniformity can come from the rf curvature, the collective effect induced microbunching instability, and also generic energy modulation in a HG FEL. We derived the bandwidth degradation to quantitatively measure this effect. The simulation and theory match reasonably well when FEL is close to the 1D limit and in the exponential growth region. We then discuss the FEL bandwidth degradation due to the generic energy modulation in a HG FEL treating the initial coherent emission as the seed into the radiator.

## ACKNOWLEDGMENTS

The work of B. Jia and Y. K. Wu was supported in part by the U.S. Department of Energy, Office of Nuclear Physics under Grant No. DE-FG02-97ER41033. The work of J. J. Bisognano was conducted at the Synchrotron Radiation Center, which is supported by National Science Foundation Award No. DMR-0537588 and the University of Wisconsin-Madison. The work of A. W. Chao and J. Wu was supported by the U.S. Department of Energy under Contract No. DE-AC02-76SF00515. This work was performed in support of the Linac Coherent Light Source project at the SLAC National Accelerator Laboratory.

[1] P. Emma, in *Proceedings of the 23rd Particle Accelerator Conference, Vancouver, Canada, 2009* (IEEE, Piscataway, NJ, 2009), TH3PBI01.
[2] N. A. Vinokurov and A. N. Skrinsky, Institute of Nuclear Physics Report No. 77-59, Novosibirsk, 1977.
[3] R. Bonifacio, L. D. S. Souza, P. Pierini, and E. T. Scharlemann, Nucl. Instrum. Methods Phys. Res., Sect. A **296**, 787 (1990).
[4] L. H. Yu, Phys. Rev. A **44**, 5178 (1991).
[5] J. Wu, P. J. Emma, R. A. Bosch, and K. J. Kleman, in Proceedings of the XXIV Linear Accelerator Conference (LINAC'08), 2008, Victoria, British Columbia, Canada, p. 512.
[6] M. Borland *et al.*, *Proceedings of the 2001 Particle Accelerator Conference* (IEEE, Piscataway, NJ, 2001), p. 2707.
[7] M. Borland *et al.*, Nucl. Instrum. Methods Phys. Res., Sect. A **483**, 268 (2002).
[8] E. Saldin, E. Schneidmiller, and M. Yurkov, Nucl. Instrum. Methods Phys. Res., Sect. A **490**, 1 (2002).
[9] S. Heifets, G. Stupakov, and S. Krinsky, Phys. Rev. ST Accel. Beams **5**, 064401 (2002).
[10] Z. Huang and K.-J. Kim, Phys. Rev. ST Accel. Beams **5**, 074401 (2002).
[11] E. Saldin, E. Schneidmiller, and M. Yurkov, Nucl. Instrum. Methods Phys. Res., Sect. A **528**, 355 (2004).
[12] Z. Huang *et al.*, Phys. Rev. ST Accel. Beams **7**, 074401 (2004).
[13] For a review of this topic, see Z. Huang, J. Wu, and T. Shaftan, ICFA Beam Dynamics Newsletter **38**, 37 (2005) [http://icfa-usa.jlab.org/archive/newsletter/icfa_bd_nl_38.pdf].
[14] M. Cornacchia *et al.*, Phys. Rev. ST Accel. Beams **9**, 120701 (2006).
[15] J. Wu, J. B. Murphy, P. J. Emma, X. Wang, T. Watanabe, and X. Zhong, J. Opt. Soc. Am. B **24**, 484 (2007).
[16] A. A. Lutman, G. Penco, P. Craievich, and J. Wu, J. Phys. A **42**, 045202 (2009).
[17] A. A. Lutman, G. Penco, P. Craievich, and J. Wu, J. Phys. A **42**, 085405 (2009).
[18] A. Marinelli, C. Pellegrini, S. Reiche, and L. Giannessi, in Proceedings of the 31st International Free Electron Laser Conference (FEL'09), 2009, Liverpool, United Kingdom, p. 31.
[19] J. Wu, A. W. Chao, and J. J. Bisognano, Proceedings of the XXIV Linear Accelerator Conference (LINAC'08), 2008, Victoria, British Columbia, Canada, p. 509.
[20] S. Reiche, Nucl. Instrum. Methods Phys. Res., Sect. A **429**, 243 (1999).

[21] L.-H. Yu *et al.*, Science **289**, 932 (2000).
[22] L. H. Yu and J. Wu, Nucl. Instrum. Methods Phys. Res., Sect. A **483**, 493 (2002).
[23] J.-M. Wang and L.-H. Yu, Nucl. Instrum. Methods Phys. Res., Sect. A **250**, 484 (1986).
[24] R. Bonifacio, C. Pellegrini, and L. M. Narducci, Opt. Commun. **50**, 373 (1984).
[25] J. B. Murphy, C. Pellegrini, and R. Bonifacio, Opt. Commun. **53**, 197 (1985).
[26] K. J. Kim, Nucl. Instrum. Methods Phys. Res., Sect. A **250**, 396 (1986).
[27] K. J. Kim, Phys. Rev. Lett. **57**, 1871 (1986).
[28] J. Wu and L. H. Yu, Nucl. Instrum. Methods Phys. Res., Sect. A **475**, 104 (2001).
[29] E. L. Saldin, E. A. Schneidmiller, and M. V. Yurkov, Opt. Commun. **202**, 169 (2002).
[30] J. Wu and L. H. Yu, SLAC Report No. SLAC-PUB-10495, 2004.
[31] S. Krinsky and L. H. Yu, Phys. Rev. A **35**, 3406 (1987).
[32] J. Wu and L. H. Yu, SLAC Report No. SLAC-PUB-10494 2004.
[33] G. E. Andrews, R. Askey, and R. Roy, *Encyclopedia of Mathematics and its Applications*, edited by G.-C. Rota (Cambridge University Press, Cambridge, England, 1999). In particular, please refer to Eq. (E.1.1) on Vol. 71, p. 629.